

# Discovery of teraelectronvolt emission from a gamma-ray burst

V. A. Acciari<sup>1</sup>, S. Ansoldi<sup>2,22</sup>, L. A. Antonelli<sup>3</sup>, A. Arbet Engels<sup>4</sup>, D. Baack<sup>5</sup>, A. Babić<sup>6</sup>, B. Banerjee<sup>7</sup>,  
U. Barres de Almeida<sup>8</sup>, J. A. Barrio<sup>9</sup>, J. Becerra González<sup>1</sup>, W. Bednarek<sup>10</sup>, L. Bellizzi<sup>11</sup>, E. Bernardini<sup>12</sup>,  
A. Berti<sup>13</sup>, J. Besenrieder<sup>14</sup>, W. Bhattacharyya<sup>12</sup>, C. Bigongiari<sup>3</sup>, A. Biland<sup>4</sup>, O. Blanch<sup>15</sup>, G. Bonnoli<sup>11</sup>,  
Ž. Bošnjak<sup>6</sup>, G. Busetto<sup>16</sup>, A. Carosi<sup>3,28</sup>, R. Carosi<sup>17</sup>, G. Ceribella<sup>14</sup>, Y. Chai<sup>14</sup>, A. Chilingaryan<sup>23</sup>,  
S. Cikota<sup>6</sup>, S. M. Colak<sup>15</sup>, U. Colin<sup>14</sup>, E. Colombo<sup>1</sup>, J. L. Contreras<sup>9</sup>, J. Cortina<sup>18</sup>, S. Covino<sup>3</sup>,  
V. D’Elia<sup>3</sup>, P. Da Vela<sup>17</sup>, F. Dazzi<sup>3</sup>, A. De Angelis<sup>16</sup>, B. De Lotto<sup>2</sup>, M. Delfino<sup>15,27</sup>, J. Delgado<sup>15,27</sup>,  
D. Depaoli<sup>13</sup>, F. Di Pierro<sup>13</sup>, L. Di Venere<sup>13</sup>, E. Do Souto Espiñeira<sup>15</sup>, D. Dominis Prester<sup>6</sup>,  
A. Donini<sup>2</sup>, D. Dorner<sup>19</sup>, M. Doro<sup>16</sup>, D. Elsaesser<sup>5</sup>, V. Fallah Ramazani<sup>20</sup>, A. Fattorini<sup>5</sup>, A. Fernández-  
Barral<sup>16</sup>, G. Ferrara<sup>3</sup>, D. Fidalgo<sup>9</sup>, L. Foffano<sup>16</sup>, M. V. Fonseca<sup>9</sup>, L. Font<sup>21</sup>, C. Fruck<sup>14</sup>, S. Fukami<sup>22</sup>,  
S. Gallozzi<sup>3</sup>, R. J. García López<sup>1</sup>, M. Garczarczyk<sup>12</sup>, S. Gasparyan<sup>23</sup>, M. Gaug<sup>21</sup>, N. Giglietto<sup>13</sup>,  
F. Giordano<sup>13</sup>, N. Godinović<sup>6</sup>, D. Green<sup>14</sup>, D. Guberman<sup>15</sup>, D. Hadasch<sup>22</sup>, A. Hahn<sup>14</sup>, J. Herrera<sup>1</sup>,  
J. Hoang<sup>9</sup>, D. Hrupec<sup>6</sup>, M. Hütten<sup>14</sup>, T. Inada<sup>22</sup>, S. Inoue<sup>22</sup>, K. Ishio<sup>14</sup>, Y. Iwamura<sup>22</sup>, L. Jouvin<sup>15</sup>,  
D. Kerszberg<sup>15</sup>, H. Kubo<sup>22</sup>, J. Kushida<sup>22</sup>, A. Lamastra<sup>3</sup>, D. Lelas<sup>6</sup>, F. Leone<sup>3</sup>, E. Lindfors<sup>20</sup>,  
S. Lombardi<sup>3</sup>, F. Longo<sup>2,26</sup>, M. López<sup>9</sup>, R. López-Coto<sup>16</sup>, A. López-Oramas<sup>1</sup>, S. Loporchio<sup>13</sup>,  
B. Machado de Oliveira Fraga<sup>8</sup>, C. Maggio<sup>21</sup>, P. Majumdar<sup>7</sup>, M. Makariev<sup>24</sup>, M. Mallamaci<sup>16</sup>,  
G. Maneva<sup>24</sup>, M. Manganaro<sup>6</sup>, K. Mannheim<sup>19</sup>, L. Maraschi<sup>3</sup>, M. Mariotti<sup>16</sup>, M. Martínez<sup>15</sup>,  
S. Masuda<sup>22</sup>, D. Mazin<sup>14,22</sup>, S. Mićanović<sup>6</sup>, D. Miceli<sup>2</sup>, M. Minev<sup>24</sup>, J. M. Miranda<sup>11</sup>, R. Mirzoyan<sup>14</sup>,  
E. Molina<sup>25</sup>, A. Moralejo<sup>15</sup>, D. Morcuende<sup>9</sup>, V. Moreno<sup>21</sup>, E. Moretti<sup>15</sup>, P. Munar-Adrover<sup>21</sup>,  
V. Neustroev<sup>20</sup>, C. Nigro<sup>12</sup>, K. Nilsson<sup>20</sup>, D. Ninci<sup>15</sup>, K. Nishijima<sup>22</sup>, K. Noda<sup>22</sup>, L. Nogués<sup>15</sup>,

22 M. Nöthe<sup>5</sup>, S. Nozaki<sup>22</sup>, S. Paiano<sup>16</sup>, J. Palacio<sup>15</sup>, M. Palatiello<sup>2</sup>, D. Paneque<sup>14</sup>, R. Paoletti<sup>11</sup>,  
 23 J. M. Paredes<sup>25</sup>, P. Peñil<sup>9</sup>, M. Peresano<sup>2</sup>, M. Persic<sup>2,27</sup>, P. G. Prada Moroni<sup>17</sup>, E. Prandini<sup>16</sup>,  
 24 I. Puljak<sup>6</sup>, W. Rhode<sup>5</sup>, M. Ribó<sup>25</sup>, J. Rico<sup>15</sup>, C. Righi<sup>3</sup>, A. Rugliancich<sup>17</sup>, L. Saha<sup>9</sup>, N. Sahakyan<sup>23</sup>,  
 25 T. Saito<sup>22</sup>, S. Sakurai<sup>22</sup>, K. Satalecka<sup>12</sup>, K. Schmidt<sup>5</sup>, T. Schweizer<sup>14</sup>, J. Sitarek<sup>10</sup>, I. Šnidarić<sup>6</sup>,  
 26 D. Sobczynska<sup>10</sup>, A. Somero<sup>1</sup>, A. Stamerra<sup>3</sup>, D. Strom<sup>14</sup>, M. Strzys<sup>14</sup>, Y. Suda<sup>14</sup>, T. Surić<sup>6</sup>, M. Takahashi<sup>22</sup>,  
 27 F. Tavecchio<sup>3</sup>, P. Temnikov<sup>24</sup>, T. Terzić<sup>6</sup>, M. Teshima<sup>14,22</sup>, N. Torres-Albà<sup>25</sup>, L. Tosti<sup>13</sup>, S. Tsujimoto<sup>22</sup>,  
 28 V. Vagelli<sup>13</sup>, J. van Scherpenberg<sup>14</sup>, G. Vanzo<sup>1</sup>, M. Vazquez Acosta<sup>1</sup>, C. F. Vigorito<sup>13</sup>, V. Vitale<sup>13</sup>,  
 29 I. Vovk<sup>14</sup>, M. Will<sup>14</sup>, D. Zarić<sup>6</sup> & L. Nava<sup>3,28,29</sup>

30 <sup>1</sup>*Inst. de Astrofísica de Canarias, E-38200 La Laguna, and Universidad de La Laguna, Dpto.*  
 31 *Astrofísica, E-38206 La Laguna, Tenerife, Spain*

32 <sup>2</sup>*Università di Udine, and INFN Trieste, I-33100 Udine, Italy*

33 <sup>3</sup>*National Institute for Astrophysics (INAF), I-00136 Rome, Italy*

34 <sup>4</sup>*ETH Zurich, CH-8093 Zurich, Switzerland*

35 <sup>5</sup>*Technische Universität Dortmund, D-44221 Dortmund, Germany*

36 <sup>6</sup>*Croatian Consortium: University of Rijeka, Department of Physics, 51000 Rijeka; University of*  
 37 *Split - FESB, 21000 Split; University of Zagreb - FER, 10000 Zagreb; University of Osijek, 31000*  
 38 *Osijek; Rudjer Boskovic Institute, 10000 Zagreb, Croatia*

39 <sup>7</sup>*Saha Institute of Nuclear Physics, HBNI, 1/AF Bidhannagar, Salt Lake, Sector-1, Kolkata 700064,*  
 40 *India*

41 <sup>8</sup>*Centro Brasileiro de Pesquisas Físicas (CBPF), 22290-180 URCA, Rio de Janeiro (RJ), Brasil*

42 <sup>9</sup>*IPARCOS Institute and EMFTEL Department, Universidad Complutense de Madrid, E-28040*

43 *Madrid, Spain*

44 <sup>10</sup>*University of Łódź, Department of Astrophysics, PL-90236 Łódź, Poland*

45 <sup>11</sup>*Università di Siena and INFN Pisa, I-53100 Siena, Italy*

46 <sup>12</sup>*Deutsches Elektronen-Synchrotron (DESY), D-15738 Zeuthen, Germany*

47 <sup>13</sup>*Istituto Nazionale Fisica Nucleare (INFN), 00044 Frascati (Roma) Italy*

48 <sup>14</sup>*Max-Planck-Institut für Physik, D-80805 München, Germany*

49 <sup>15</sup>*Institut de Física d'Altes Energies (IFAE), The Barcelona Institute of Science and Technology  
50 (BIST), E-08193 Bellaterra (Barcelona), Spain*

51 <sup>16</sup>*Università di Padova and INFN, I-35131 Padova, Italy*

52 <sup>17</sup>*Università di Pisa, and INFN Pisa, I-56126 Pisa, Italy*

53 <sup>18</sup>*Centro de Investigaciones Energéticas, Medioambientales y Tecnológicas, E-28040 Madrid,  
54 Spain*

55 <sup>19</sup>*Universität Würzburg, D-97074 Würzburg, Germany*

56 <sup>20</sup>*Finnish MAGIC Consortium: Finnish Centre of Astronomy with ESO (FINCA), University of  
57 Turku, FI-20014 Turku, Finland; Astronomy Research Unit, University of Oulu, FI-90014 Oulu,  
58 Finland*

59 <sup>21</sup>*Departament de Física, and CERES-IEEC, Universitat Autònoma de Barcelona, E-08193 Bel-  
60 laterra, Spain*

61 <sup>22</sup>*Japanese MAGIC Consortium: ICRR, The University of Tokyo, 277-8582 Chiba, Japan; Depart-  
62 ment of Physics, Kyoto University, 606-8502 Kyoto, Japan; Tokai University, 259-1292 Kanagawa,  
63 Japan; RIKEN, 351-0198 Saitama, Japan*

<sup>23</sup>*ICRANet-Armenia at NAS RA, 0019 Yerevan, Armenia*

<sup>24</sup>*Inst. for Nucl. Research and Nucl. Energy, Bulgarian Academy of Sciences, BG-1784 Sofia, Bulgaria*

<sup>25</sup>*Universitat de Barcelona, ICCUB, IEEC-UB, E-08028 Barcelona, Spain*

<sup>26</sup>*also at Dipartimento di Fisica, Università di Trieste, I-34127 Trieste, Italy*

<sup>27</sup>*also at Port d'Informació Científica (PIC) E-08193 Bellaterra (Barcelona) Spain*

<sup>28</sup>*now at Laboratoire d'Annecy de Physique des Particules, Univ. Grenoble Alpes, Univ. Savoie Mont Blanc, CNRS, LAPP, 74000 Annecy, France*

<sup>29</sup>*Istituto Nazionale Fisica Nucleare (INFN), I-34149 Trieste, Italy*

<sup>30</sup>*Institute for Fundamental Physics of the Universe (IFPU), I-34151 Trieste, Italy*

**Gamma-ray bursts (GRBs) of the long-duration class are the most luminous sources of electromagnetic radiation known in the Universe, triggered by outflows of plasma ejected at near the speed of light by newly formed neutron stars or black holes of stellar mass at cosmological distances<sup>1,2</sup>. Prompt flashes of MeV gamma rays are followed by longer-lasting afterglow emission from radio waves to GeV gamma rays, due to synchrotron radiation by energetic electrons in accompanying shock waves<sup>3,4</sup>. Although emission of higher energy, TeV gamma rays due to other radiation mechanisms had been theoretically predicted in some studies<sup>5-9</sup>, it had never been detected previously, despite numerous attempts to search for them<sup>8,9</sup>. Here we report the discovery of GRB 190114C with the Major Atmospheric Gamma Imaging Cherenkov (MAGIC) telescopes<sup>10,11</sup>, the first GRB to be clearly detected in the TeV band after 15 years of dedicated searches. Gamma rays in the energy range 0.3–1 TeV are detected**

with very high significance from about 1 minute after the burst (at more than 50 standard deviations in the first 20 minutes). These are by far the highest energy photons ever detected from a GRB, with initial flux and luminosity above 0.3 TeV much higher than any previously known source. For the first time, this unambiguously reveals a new emission component in the afterglow of a GRB, whose power is comparable to that of the synchrotron component.

GRB 190114C was first identified as a long-duration GRB by the BAT instrument onboard the Neil Gehrels Swift Observatory (*Swift*)<sup>12</sup> and the Gamma-ray Burst Monitor (GBM) instrument onboard the *Fermi* satellite<sup>13</sup> on 14 January 2019, 20:57:03 Universal Time (UT) (hereafter  $T_0$ ). Soon afterwards, reports followed on the detection of its afterglow emission at various wavebands from 1.3 GHz up to 23 GeV (Acciari et al., in preparation) and the measurement of its redshift  $z = 0.4245 \pm 0.0005$ <sup>14,15</sup> (corresponding to cosmic distance). In the energy range  $\varepsilon = 1 - 1000$  keV, GRB 190114C was fairly energetic, but not exceptionally so compared to previous events (Methods).

MAGIC is a system of two 17m diameter imaging atmospheric Cherenkov telescopes, with the design optimised to search for GRBs as a primary goal, along with many other scientific objectives<sup>11</sup> (Methods). Triggered by the *Swift*/BAT alert, the MAGIC telescopes observed GRB 190114C from  $T_0 + 57$  seconds until  $T_0 + 15912$  seconds (Extended Data Fig.1). Gamma rays above 0.3 TeV were detected with high significance from the beginning of the observations<sup>16</sup>; in the first 20 minutes of data, the significance of the total gamma-ray signal is more than 50 standard

deviations (Methods, Extended Data Fig. 2). These are the highest energy photons ever detected from a GRB, and mark the very first time that a GRB is unambiguously detected above 100 GeV. It is also the brightest source to date at 0.3 TeV, with flux about 100 times higher than from the Crab Nebula during the first 30 seconds of observations.

For cosmologically distant objects such as GRBs, the observed gamma-ray spectra are substantially modified due to attenuation by the extragalactic background light (EBL)<sup>17</sup>. The EBL is the diffuse background of infrared, optical and ultraviolet radiation that permeates intergalactic space, constituting the emission from all galaxies in the Universe. Gamma rays can be effectively absorbed during their propagation via photon-photon pair production interactions with low-energy photons of the EBL, which is more severe for higher photon energies and higher redshifts. The gamma-ray spectrum that would be observed if the EBL was absent, referred to as the intrinsic spectrum, can be inferred from the observed spectrum by “correcting” for EBL attenuation, assuming a plausible model of the EBL<sup>18</sup>.

Emission from GRBs occurs in two stages that can partially overlap in time. The “prompt” emission phase is characterised by a brief but intense flash of gamma rays, primarily at MeV energies, that exhibit irregular variability on timescales shorter than milliseconds, and last up to hundreds of seconds for long-duration GRBs. These gamma rays are generated in the inner regions of collimated jets of plasma, which are ejected with ultra-relativistic velocities from highly magnetised neutron stars or black holes that form following the death of massive stars<sup>2</sup>. The ensuing “afterglow” phase is characterised by emission that spans a very broad wavelength range

and decays gradually over much longer timescales. This originates from shock waves caused by the interaction of the jet with the ambient gas (“external shocks”), whose evolution is typified by power-law decay in time due to the self-similar properties of the decelerating shock wave<sup>3,4</sup>. The afterglow emission of previously observed GRBs from radio frequencies to GeV energies is generally interpreted as synchrotron radiation from energetic electrons that are accelerated within magnetised plasma at the external shock<sup>2</sup>. Clues to whether the newly observed TeV emission is associated with the prompt or the afterglow phase are offered by the observed light curve (flux  $F(t)$  as a function of time  $t$ ).

Fig. 1 shows such a light curve for the EBL-corrected intrinsic flux in the energy range  $\varepsilon = 0.3 - 1$  TeV (see also Extended Data Table 1). It is well fit with a simple power-law function  $F(t) \propto t^\beta$  with  $\beta = -1.56 \pm 0.08$ . The flux evolves from  $F(t) \sim 5 \times 10^{-8} \text{ erg cm}^{-2} \text{ s}^{-1}$  at  $t \sim T_0 + 80 \text{ s}$  to  $F(t) \sim 6 \times 10^{-10} \text{ erg cm}^{-2} \text{ s}^{-1}$  at  $t \gtrsim T_0 + 10^3 \text{ s}$ , after which it falls below the sensitivity level and is undetectable. There is no clear evidence for breaks or cutoffs in the light curve, nor irregular variability beyond the monotonic decay. The light curves in the keV and GeV bands display behaviour similar to the TeV band, with somewhat shallower decay slope for the GeV band (Fig. 1). These properties indicate that most of the observed emission is associated with the afterglow phase, rather than the prompt phase that typically shows irregular variability. Note, however, that a sub-dominant contribution at early times from the prompt phase cannot be excluded. The flux initially observed at  $t \sim T_0 + 80 \text{ s}$  corresponds to apparent isotropic-equivalent luminosity  $L_{\text{iso}} \sim 3 \times 10^{49} \text{ erg s}^{-1}$  at  $\varepsilon = 0.3 - 1$  TeV, making this the most luminous source known above 0.3 TeV.

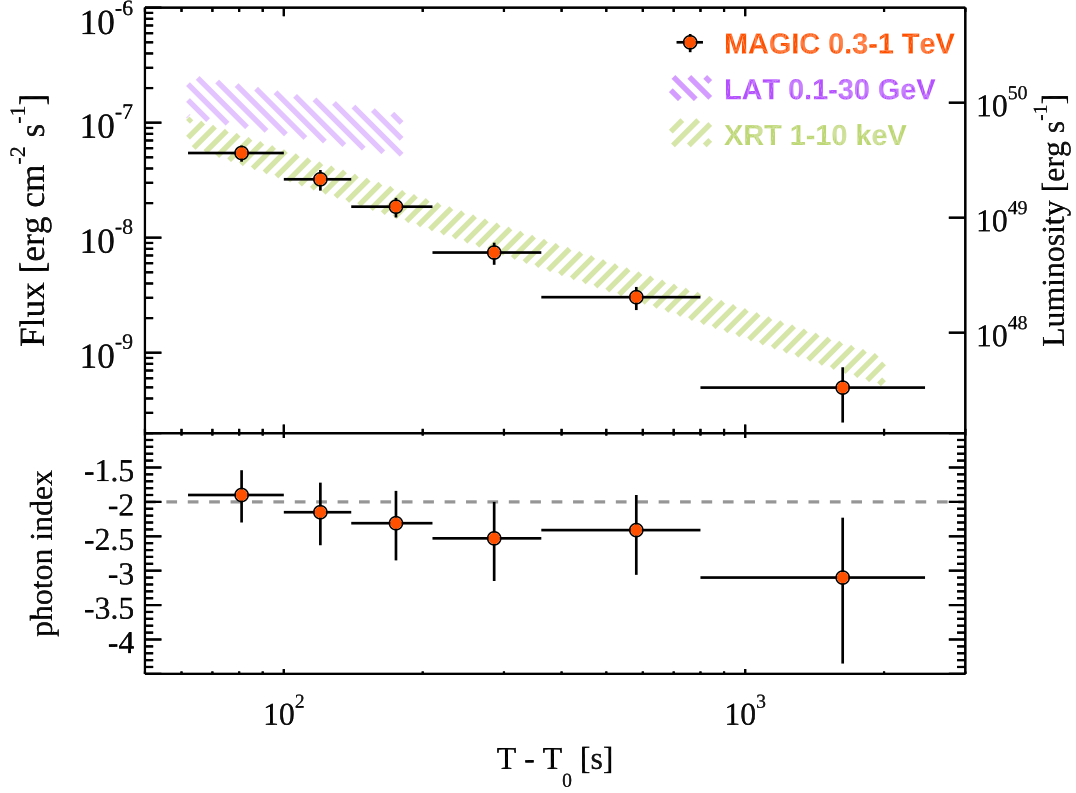


Figure 1: **Light curves in the keV, GeV and TeV bands, and spectral evolution in the TeV band for GRB 190114C.** Top panel: Light curves in units of energy flux (left axis) or apparent luminosity (right axis), for MAGIC at 0.3 – 1 TeV (red symbols), *Fermi*/LAT at 0.1 – 30 GeV (purple band) and *Swift*/XRT at 1 – 10 keV (green band). For MAGIC, the intrinsic flux is shown, corrected for EBL attenuation<sup>18</sup> from the observed flux. Bottom panel: Temporal evolution of the power-law photon index determined from time-resolved intrinsic spectra at 0.3 – 1 TeV. The horizontal dashed line indicates the value -2. The errors shown in both panels are statistical only.

The power radiated in the TeV band is comparable to that in the soft X-ray band, and is a sizable fraction ( $\sim 30\%$ ) of that in the GeV band, during the periods when simultaneous TeV-keV or TeV-GeV data are available (Fig. 1). The energy radiated at  $\varepsilon = 0.3 - 1$  TeV integrated over the



time period between  $T_0 + 62$  seconds and  $T_0 + 2454$  seconds is  $E_{0.3-1 \text{ TeV}} \sim 3 \times 10^{51}$  erg, which is a lower limit to the total TeV-band output, as it does not account for data before  $T_0 + 62$  seconds, nor the strongly attenuated emission at  $\varepsilon > 1$  TeV. Assuming that the MAGIC light curve evolved as  $F(t) \propto t^{-1.56}$  from  $t \sim T_0 + 6$  s, the start of the power-law decay phase inferred from MeV-GeV data<sup>19,20</sup>, the TeV-band energy output would be  $E_{0.3-1 \text{ TeV}} \sim 2 \times 10^{52}$  erg, which is  $\sim 10\%$  of  $E_{\text{iso}}$ , the isotropic-equivalent energy of the prompt emission at  $\varepsilon = 10\text{--}1000$  keV.

Fig. 1 also shows the time evolution of the intrinsic spectral photon index  $\alpha_{\text{int}}$ , determined by fitting the EBL-corrected, time-dependent differential photon spectrum above 0.3 TeV with the power-law function  $dF/d\varepsilon \propto \varepsilon^{\alpha_{\text{int}}}$ . Throughout the observations, the data are consistent with  $\alpha_{\text{int}} = -2$  within the uncertainties, indicating that the radiated power is nearly equally distributed in  $\varepsilon$  over this band.

Fig. 2 presents both the observed and the EBL-corrected intrinsic flux spectra above 0.2 TeV, averaged over  $(T_0 + 62 \text{ s}, T_0 + 2454 \text{ s})$  when the GRB is detectable by MAGIC. The former can be fit in the energy range  $0.2 - 1$  TeV with a simple power-law with photon index  $\alpha_{\text{obs}} = -5.27 \pm 0.30$  (statistical error only), one of the steepest spectra ever observed for a gamma-ray source. It is remarkable that photons are clearly detected at  $\varepsilon \sim 1$  TeV, despite the severe EBL attenuation expected at these energies (by a factor  $\sim 300$  based on a plausible EBL model<sup>18</sup>). The intrinsic spectrum is well described with a power-law with  $\alpha_{\text{int}} = -2.22_{-0.25}^{+0.23}$  (statistical error only), without any evidence for a spectral break or cutoff. Since the value of  $\alpha_{\text{int}}$  is not far from  $-2$ , this implies roughly equal power radiated over  $0.2 - 1$  TeV and possibly beyond, which strengthens

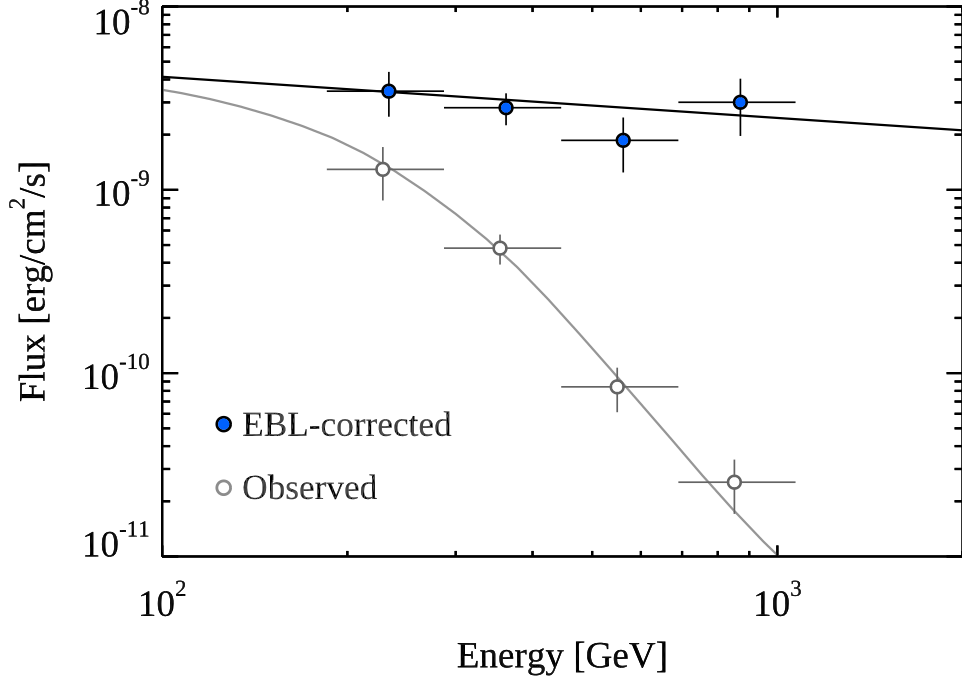


Figure 2: **Spectrum above 0.2 TeV averaged over the period between  $T_0+62$  s and  $T_0+2454$  s for GRB 190114C.** Spectral energy distributions for the spectrum observed by MAGIC (grey open circles) and the intrinsic spectrum corrected for EBL attenuation<sup>18</sup> (blue filled circles). Also shown are the best fit models for the observed spectrum (grey curve) and intrinsic spectrum (black curve), when assuming a power-law form for the intrinsic spectrum (Methods).

the inference that there is significant energy output at TeV energies.

Much of the observed emission up to GeV energies for GRB 190114C is likely afterglow synchrotron emission from electrons, similar to many previous GRBs<sup>2,21</sup>. The TeV emission observed here is also plausibly associated with the afterglow. However, it cannot be a simple spectral extension of the electron synchrotron emission. The maximum energy of the emitting

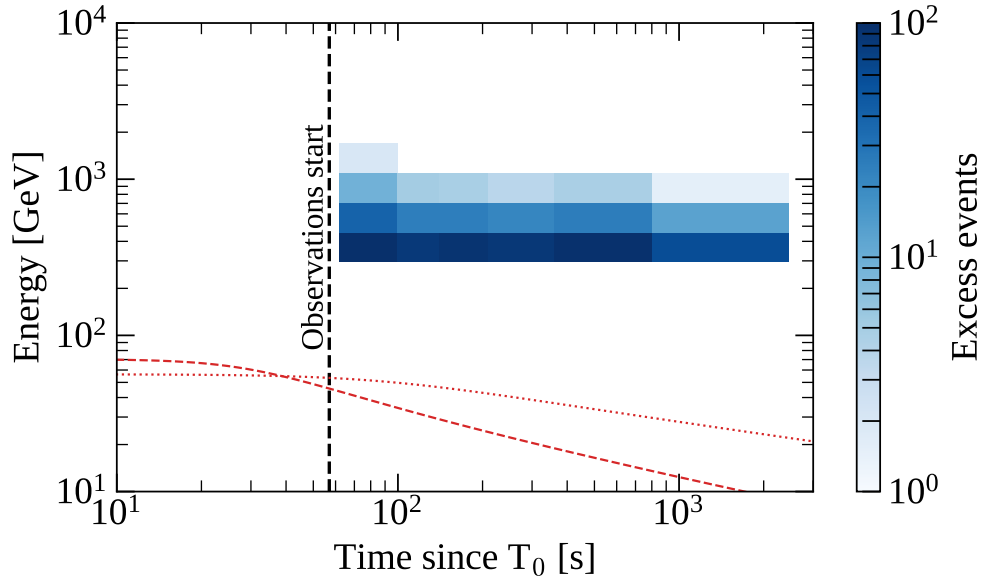


Figure 3: **Distribution of TeV-band gamma rays in energy versus time for GRB 190114C.**

The number of photons detected by MAGIC in each bin of energy and time are color-coded. The vertical line indicates the beginning of data acquisition. Curves show the expected maximum photon energy  $\varepsilon_{\text{syn,max}}$  of electron synchrotron radiation in the standard afterglow theory, for two extreme cases giving high values of  $\varepsilon_{\text{syn,max}}$ . Dotted curve: blast wave kinetic energy  $E_{\text{k,aft}} = 3 \times 10^{55}$  erg and homogeneous external medium with density  $n = 0.01 \text{ cm}^{-3}$ ; dashed curve:  $E_{\text{k,aft}} = 3 \times 10^{55}$  erg and external medium describing a progenitor stellar wind with density profile  $n(R) = AR^{-2}$  as function of radius  $R$ , where  $A = 3 \times 10^{33} \text{ cm}^{-1}$  (Methods).

174 electrons is determined by a balance between their energy losses dominated by synchrotron ra-  
 175 diation, and their acceleration whose timescale should not be much shorter than the timescale  
 176 of their gyration around the magnetic field at the external shock. The energy of afterglow syn-  
 177 chrotron photons is then limited to a maximum value, the so-called synchrotron burnoff limit<sup>22,23</sup>

178 of  $\varepsilon_{\text{syn,max}} \sim 100(\Gamma_b/1000)$  GeV, which depends only on the bulk Lorentz factor that is unlikely  
 179 to significantly exceed  $\Gamma_b \sim 1000$  (Methods). Fig. 3 compares the observed photon energies with  
 180 expectations of  $\varepsilon_{\text{syn,max}}$  under different assumptions. Although a few gamma rays with energy  
 181 approaching  $\varepsilon_{\text{syn,max}}$  had been previously detected from a GRB by *Fermi*<sup>23</sup>, the evidence for a  
 182 separate spectral component was not conclusive, given the uncertainties in  $\Gamma_b$ , electron accelera-  
 183 tion rate, and the spatial structure of the emitting region<sup>24</sup>. Here, even the lowest energy photons  
 184 detected by MAGIC are significantly above  $\varepsilon_{\text{syn,max}}$  and extend beyond 1 TeV at 95% confidence  
 185 level. Thus, these observations provide the first unequivocal evidence for a new emission compo-  
 186 nent beyond synchrotron emission in the afterglow of a GRB. Moreover, this component is ener-  
 187 getically important, with power nearly comparable to that in the synchrotron component observed  
 188 contemporaneously.

189 Comparing with previous MAGIC observations of GRBs, the fact that GRB 190114C was  
 190 the first to be clearly detected is likely due to a favourable combination of its low redshift and the  
 191 capability to observe at partial Moon light and at relatively large zenith angle range, rather than  
 192 its intrinsic properties being exceptional (Methods). The discovery of an energetically important  
 193 emission component beyond synchrotron emission that may be common in GRB afterglows of-  
 194 fers crucial new insight into the physics of GRBs. A promising origin of the observed TeV-band  
 195 gamma-rays is synchrotron-self-Compton (SSC) radiation from the afterglow, in which low-energy  
 196 synchrotron photons emitted by electrons at the external shock are Compton upscattered to high  
 197 energies by the same population of electrons<sup>25–27</sup>. To produce TeV gamma rays as luminous as  
 198 observed via the SSC mechanism, the magnetic field strength at the external shock must likely

199 be considerably lower than inferred from many earlier afterglow models based on observations of  
200 the synchrotron emission alone<sup>27</sup> (Acciari et al., in preparation). Thanks to the extremely strong  
201 signal these observations may also provide new information concerning the EBL and the validity  
202 of special relativity<sup>8</sup>.

203 Although long anticipated, the detection of TeV gamma rays from GRBs had been an ex-  
204 tremely challenging endeavour. It was finally realised here with very high significance for the first  
205 time, after many years of technical improvements and dedicated efforts. Despite the numerous ear-  
206 lier non-detections, most GRBs may actually possess TeV emission components similar to GRB  
207 190114C, which are detectable as long as their redshift is low and the observing conditions are  
208 suitable. Continuing efforts with existing gamma-ray telescopes, as well as the new Cherenkov  
209 Telescope Array currently under construction<sup>28</sup>, promise to bring forth new physical insight into  
210 the most luminous electromagnetic explosions in the Universe.

## Methods

**General properties of GRB 190114C.** GRB 190114C was first identified by the *Swift*/BAT<sup>12</sup> and *Fermi*/GBM<sup>13</sup> instruments on 14 January 2019, 20:57:03 UT. Subsequently, it was also detected by several other space-based instruments, including *Fermi*/LAT, *INTEGRAL*/SPI-ACS, *AGILE*/MCAL, *Insight*/HXMT and Konus-Wind<sup>20</sup>. Its redshift was reported as  $z = 0.4245 \pm 0.0005$  by the Nordic Optical Telescope<sup>14</sup> and confirmed by Gran Telescopio Canarias<sup>15</sup>. The fluence and peak photon flux of the prompt emission at 10 – 1000 keV measured by GBM are  $(3.990 \pm 0.008) \times 10^{-4} \text{ erg cm}^{-2}$  and  $(246.86 \pm 0.86) \text{ ph cm}^{-2} \text{ s}^{-1}$ <sup>13</sup>, corresponding to  $E_{\text{iso}} \sim 3 \times 10^{53} \text{ erg}$  and  $L_{\text{iso}} \sim 1 \times 10^{53} \text{ erg s}^{-1}$ , respectively<sup>20</sup>. These values are consistent with the known correlations for GRBs between their spectral peak energy  $\varepsilon_{\text{peak}}$  and  $E_{\text{iso}}$ <sup>29</sup>, and between  $\varepsilon_{\text{peak}}$  and  $L_{\text{iso}}$ <sup>30</sup>. The light curve of the prompt emission exhibits two main emission episodes with multi-peak structure. Its duration in terms of  $T_{90}$  (time interval containing 90% of the total photon counts) is  $\sim 6 - 360$  sec depending on the energy range<sup>13,31</sup>, putting GRB 190114C unambiguously in the long-duration subclass of GRBs<sup>1</sup>. The event is fairly energetic but not exceptionally so, with  $E_{\text{iso}}$  lying in the highest  $\sim 30\%$  of its known distribution<sup>32</sup>. No neutrinos were detected by the IceCube Observatory in the energy range 100 TeV to 10 PeV, under non-optimal observing conditions<sup>33</sup>.

**MAGIC Telescopes and Automatic Alert System.** The MAGIC telescopes comprise two 17-m diameter IACTs (MAGIC-I and MAGIC-II) operating in stereoscopic mode, located at the Roque de los Muchachos Observatory in La Palma, Canary Islands, Spain<sup>10,11</sup>. By imaging Cherenkov light from extended air shower events, the telescopes can detect gamma rays above an energy threshold of 30 GeV depending on the observing mode and conditions, with a field of view of  $\sim 10$

square degrees.

Observing GRBs with IACTs such as MAGIC warrants a dedicated strategy. As the probability of discovering GRBs by IACTs serendipitously in their relatively small field of view is relatively low, they rely on external alerts provided by satellite instruments to trigger follow-up observations. Since their inception, the MAGIC telescopes were designed to perform fast follow-up observations of GRBs. By virtue of their light-weight reinforced carbon fiber structure and high repositioning speed in the so-called fast mode, they can respond quickly to GRB alerts received via the Gamma-ray Coordinates Network (GCN<sup>1</sup>)<sup>34</sup>. After various updates to the entire system over the years<sup>10,11</sup>, the telescopes can currently slew to a target with a repositioning speed of 7 degrees per second. To achieve the fastest possible response to GRB alerts, an Automatic Alert System (AAS) has been developed, which is a multi-threaded program that performs different tasks such as connecting to the GCN servers, receiving GCN Notices that contain the sky coordinates of the GRB, and sending commands to the Central Control (CC) software of the MAGIC telescopes. This also includes a check of the visibility of the new target according to predefined criteria. A priority list was set up for cases when several different types of alerts are received simultaneously. Moreover, if there are multiple alerts for the same GRB, the AAS will select the one with the best localization.

If an alert is tagged as observable by the AAS, the telescopes will automatically repoint to the new sky position. An automatic procedure, implemented in 2013, prepares the subsystems for data taking during the telescope slewing<sup>35,36</sup>: previously taken data is saved, relevant trigger tables

---

<sup>1</sup><https://gcn.gsfc.nasa.gov>

are loaded, appropriate electronics thresholds are set and the mirror segments are suitably adjusted by the Automatic Mirror Control hardware. While moving, the telescopes calibrate the imaging cameras. The Data Acquisition (DAQ) system continues taking data while it receives information about the target from the CC software. The presence of a trigger limiter set to 1 kHz prevents high rate values and the saturation of the DAQ system. When the repositioning has finished, the target is tracked in wobble mode, which is the standard observing mode for MAGIC<sup>37</sup>. To date, the fastest GRB follow-up was achieved for GRB 160821B, when the data taking started only 24 seconds after the GRB.

**MAGIC observations of GRB 190114C.** On the night of 14 January 2019, at 20:57:25 UT ( $T_0 + 22$  s), *Swift*/BAT distributed an alert reporting the first estimated coordinates of GRB 190114C (RA: +03h 38m 02s; Dec: -26d 56m 18s). The AAS validated it as observable and triggered the automatic repointing procedure, and the telescopes began slewing in fast mode from the target position before the alert. The MAGIC-I and MAGIC-II telescopes were on target and began tracking GRB 190114C at 20:57:52.858 UT and 20:57:53.260 UT ( $T_0 + 50$  s), respectively, starting from zenith angle  $55.8^\circ$  and azimuth angle  $175.1^\circ$  in local coordinates. After starting the slewing, the telescopes reached the target position in approximately 27 seconds, moving by 42.82 degrees in zenith and 177.5 degrees in azimuth. At the end of the slewing, the cameras on the telescopes oscillated for a short time. Subsequently, we performed a dedicated test that reproduced the movement of the telescopes, and verified that the duration of the oscillations was less than 10 seconds after the start of tracking, and its amplitude was less than 0.6 arc-minutes when data taking began. Data acquisition started at 20:58:00 ( $T_0 + 57$  s) and the DAQ system was operating stably from



273 20:58:05 ( $T_0 + 62$  s), as denoted in Extended Data Fig. 1.

274 Observations were performed in the presence of moonlight, implying a relatively high night  
275 sky background (NSB), approximately  $\sim 6$  times the level for dark observations (moonless nights  
276 with good weather conditions)<sup>38</sup>. Data taking for GRB 190114C stopped on 15 January 2019,  
277 01:22:15 UT, when the target reached zenith angle  $81.14^\circ$  and azimuth angle  $232.6^\circ$ . The total  
278 exposure time for GRB 190114C was 4.12 h.

279 **MAGIC data analysis for GRB 190114C.** Data collected for GRB 190114C were analysed using  
280 the standard MAGIC analysis software<sup>11</sup> and the analysis chain tuned for data taken under moon-  
281 light conditions<sup>38</sup>. No detailed information on the atmospheric transmission is available since the  
282 LIDAR facility<sup>39</sup> was not operating during the night of the observation. Therefore, the quality of  
283 the data was assessed by checking the value and stability of the DAQ rates, as well as reports from  
284 the observers at the MAGIC site.

285 A dedicated set of Monte Carlo (MC) simulation gamma-ray data was produced for the  
286 analysis, matching the trigger settings (discriminator thresholds), the zenith-azimuth distribution,  
287 and the NSB level of GRB 190114C observations. The final data set comprises events starting  
288 from 20:58:05 UT. Due to the higher NSB, compared to standard analysis, a higher level of image  
289 cleaning was applied to both real and MC data, while a higher cut on the integrated charge of the  
290 event image, set to 80 photo-electrons, was used for evaluating photon fluxes<sup>38</sup>. The significance  
291 of the gamma-ray signal was computed using the Li & Ma method<sup>40</sup>.

292 The spectra in Figure 2 were derived by assuming a simple power law form for the intrinsic

spectrum,

$$\frac{dF}{d\varepsilon} = f_0 \times \left( \frac{\varepsilon}{\varepsilon_0} \right)^{-\alpha},$$

with the forward-folding method to derive the best fit parameters and the Schmelling unfolding prescription for the spectral points<sup>41</sup>, starting from the observed spectrum and correcting for EBL attenuation with the model of Dominguez et al.<sup>18</sup>. The best fit values are  $\alpha_{\text{int}} = -2.22^{+0.23}_{-0.25} \text{ (stat)}^{+0.21}_{-0.26} \text{ (sys)}$  and  $f_{0,\text{int}} = [8.45^{+0.68}_{-0.65} \text{ (stat)}^{+4.42}_{-3.97} \text{ (sys)}] \cdot 10^{-9} \text{ TeV}^{-1} \text{ cm}^{-2} \text{ s}^{-1}$  at 0.45 TeV. Note that due to the soft spectrum of the source, the systematic errors reported here are larger than the ones given in Aleksic et al.<sup>11</sup> and derive from the uncertainty on the knowledge of the absolute instrument calibration and of the atmospheric transmission. The results are similar with those obtained with other currently available EBL models<sup>42</sup> at the redshift of this GRB. The observed spectrum in the 0.2 – 1.0 TeV energy range can be roughly described by a power-law with photon index  $\alpha_{\text{obs}} = -5.27 \pm 0.30 \text{ (stat)}$  and flux normalization  $f_{0,\text{obs}} = [4.88 \pm 0.50 \text{ (stat)}] \cdot 10^{-10} \text{ TeV}^{-1} \text{ cm}^{-2} \text{ s}^{-1}$  at 0.45 TeV.

The time-dependent, EBL-corrected energy flux in Figure 1 and Table 1 was computed with a toy Monte Carlo simulation. For each time bin, random samples for the normalization and spectral photon index were generated according to the forward folding best-fit parameters, errors and correlation matrix. For each pair of values for normalization and index, a value for the energy flux was computed by integrating the corresponding spectral model between 0.3 and 1 TeV, obtaining a distribution of values. The final values for the EBL-corrected energy flux and its error are given by the mean and standard deviation of this distribution.

The lower limits on the maximum event energy were computed by an iterative procedure

where a power-law model is assumed for the intrinsic spectrum, and a different cut is applied to the maximum event energy for each iteration. For each value of the energy cut, a forward-folding fit is performed and a  $\chi^2$  value is obtained. The final result is obtained by finding the value of the energy cut for which the  $\chi^2$  variation corresponds to a given confidence level, set here to 95%.

The number of excess events in each time bin was computed by using the forward-folding the EBL-corrected spectrum, the instrument effective area and the effective time of the observation.

**Fermi/LAT data analysis for GRB 190114C.** The publicly available Pass 8 (P8R3) LAT data for GRB 190114C was processed using the Conda fermitools v1.0.2 package, distributed by the Fermi collaboration<sup>2</sup>. Events of the “Transient” class (P8R3\_TRANSIENT020\_V2) were selected within  $10^\circ$  from the source position. We assumed a power law spectrum in the  $0.1 - 30$  GeV energy range, also accounting for the diffuse galactic and extragalactic backgrounds, as described in the analysis manual<sup>3</sup>. To compute the source fluxes, we first checked that the spectral index is consistent with  $-2$  for the entire 62–200 seconds interval after  $T_0$ , and then repeated the fit, fixing the index to this value. The LAT energy flux shown in Fig. 1 was computed as the integral of the best-fit power law model within the corresponding energy range.

**XRT lightcurve.** The XRT lightcurve shown in Fig.1 was derived from the online analysis tool that is publicly available at the *Swift*-XRT repository<sup>4</sup>. The spectral data collected in the Windowed Timing (WT) mode suffered from an instrumental effect, causing a non-physical excess

---

<sup>2</sup><https://fermi.gsfc.nasa.gov/ssc/data/analysis/software/>

<sup>3</sup><https://fermi.gsfc.nasa.gov/ssc/data/analysis/scitools/>

<sup>4</sup>[http://www.swift.ac.uk/xrt\\_curves/](http://www.swift.ac.uk/xrt_curves/)

of counts below  $\sim 0.8 \text{ keV}^{43}$ . To remove this effect, we considered the best fit model of spectral data above 1 keV and estimated a conversion factor from counts to deabsorbed flux equal to  $10^{-10} \text{ erg cm}^{-2} \text{ ct}^{-1}$ . This conversion factor was applied to the counts lightcurve to derive the energy flux light curve in the time interval 62-2000 s.

**Synchrotron burnoff limit for the afterglow emission.** GRB afterglows are triggered by external shocks that decelerate and dissipate their kinetic energy in the ambient medium, consequently producing a nonthermal distribution of electrons via mechanisms such as shock acceleration<sup>2</sup>. The maximum energy of electrons that can be attained in the reference frame comoving with the post-shock region can be estimated by equating the timescales of acceleration  $\tau_{\text{acc}}$  and energy loss  $\tau_{\text{loss}}$ , the latter primarily due to synchrotron radiation<sup>22</sup>. These are expected to scale with electron Lorentz factor  $\gamma$  and magnetic field strength  $B$  as  $\tau_{\text{acc}} \propto \gamma B^{-1}$  and  $\tau_{\text{loss}} \propto \gamma^{-1} B^{-1}$ , so that the maximum electron Lorentz factor  $\gamma_{\text{max}} \propto B^{-1/2}$ . Thus, the maximum energy of synchrotron emission  $\varepsilon_{\text{syn,max}} \propto B \gamma_{\text{max}}^2$  is independent of  $B$ . Its numerical value in the shock comoving frame is  $\varepsilon'_{\text{syn,max}} \sim 50 - 100 \text{ MeV}$ , determined only by fundamental constants and a factor of order one that characterizes uncertainties in the acceleration timescale. The observed spectrum of afterglow synchrotron emission is then expected to display a cutoff below the energy  $\varepsilon_{\text{syn,max}} \sim 100 \text{ MeV} \times \Gamma_b(t)/(1+z)$ , which depends only on the time-dependent bulk Lorentz factor  $\Gamma_b(t)$  of the external shock. To estimate  $\varepsilon_{\text{syn,max}}$  and its evolution, we employ  $\Gamma_b(t)$  derived from solutions to the dynamical equations of the external shock<sup>44</sup>. The resulting curves for  $\varepsilon_{\text{syn,max}}$  are shown for cases of a medium with constant density  $n = \text{const}$ , and a medium with a radial density profile  $n(R) = A R^{-2}$  (with  $A = 3 \times 10^{35} A_\star \text{ cm}^{-1}$ ), expected when a dense stellar wind is produced by

the progenitor star (dotted and dashed lines in Figure 3, respectively). These curves have assumed small values for the density ( $n = 0.01$  and  $A_\star = 0.01$ ) and the efficiency of prompt emission ( $\eta_\gamma = 1\%$ ) that implies a large value for the blastwave kinetic energy ( $E_{k,\text{aft}} = E_{\text{iso}}(1 - \eta_\gamma)/\eta_\gamma$ ), resulting in high values of  $\varepsilon_{\text{syn,max}}$ . Even with such extreme assumptions, the energy of photons detected by MAGIC are well above  $\varepsilon_{\text{syn,max}}$  (Fig.3).

**Past TeV-band observations of GRBs with MAGIC and other facilities.** The search for TeV gamma rays from GRBs had been pursued over many years employing a variety of experimental techniques, but no clear detections had been previously achieved<sup>45–56</sup>.

Designed with GRB follow-up observations as a primary goal, MAGIC has been responding to GRB alerts since 15th July 2004. For the first 5 years, MAGIC operated with a single telescope (MAGIC-I), reacting mainly to alerts from *Swift*. After the second telescope (MAGIC-II) was added in 2009, GRB observations have been carried out in stereoscopic mode. Excluding cases when proper data could not be taken due to hardware problems or weather conditions, 105 GRBs were observed from July 2004 to February 2019. Of these, 40 have determined redshifts, among which 8 and 3 have redshifts lower than 1 and 0.5, respectively. Observations started less than 30 minutes after the burst for 66 events (of which 33 lack redshifts), and less than 60 seconds for 14 events. The small number of the latter is mainly due to bad weather conditions or observational criteria that were not fulfilled at the time of the alert.

Despite 15 years of dedicated efforts, no unambiguous evidence for gamma-ray signals from GRBs had been seen by MAGIC before GRB 190114C. The flux upper limits for GRBs observed in

2005-2006 were found to be consistent with simple power-law extrapolations of their low-energy spectra when EBL attenuation was taken into account<sup>57</sup>. More detailed studies were presented for GRB 080430<sup>58</sup> and GRB 090102<sup>59</sup> that were simultaneously observed with MAGIC and other instruments in different energy bands. Since 2013, GRB observations have been performed with the new automatic procedure described above<sup>35,36</sup>. In addition, for some bright GRBs detected by Fermi/LAT, late-time observations have been conducted up to one day after the burst to search for potential signals extended in time.

The case of GRB 190114C can be compared with other GRBs followed up by MAGIC under similar conditions. Aside from the intrinsic spectrum, the main factors affecting the detectability of a GRB by IACTs are the redshift  $z$  (stronger EBL attenuation for higher  $z$ ), the zenith distance (higher energy threshold for higher zenith distance), outside light conditions and the delay time  $T_{\text{delay}}$  between the GRB and the beginning of the observations. If we select GRBs with  $z < 1$  and  $T_{\text{delay}} < 1$  h, only four events remain, as listed in Table 2. Except for GRB 190114C, these are all short GRBs, which is not surprising as they are known to be distributed at redshifts appreciably lower than long GRBs<sup>60</sup>. A few other long GRBs with  $z < 1$  were actually followed up by MAGIC with  $T_{\text{delay}} < 1$  h, but the observations were not successful due to technical problems or adverse observing conditions. There is also a fair fraction of events without measured redshifts. Assuming that they follow the known  $z$  distribution of long GRBs,  $\sim 20\%$  of the events are expected at  $z < 1$ <sup>61</sup>. Since 30 long GRBs without redshifts were observed by MAGIC with  $T_{\text{delay}} < 1$  h, the total number of events with observing conditions and  $z$  similar to GRB 190114C during the whole MAGIC GRB campaign is likely to be only a few. Thus, the fact that GRB 190114C was the first

clear GRB detection by MAGIC is consistent with being mainly due to the favourable combination of its distance and the observing conditions, rather than the event being particularly exceptional in terms of its intrinsic properties.

1. Gehrels, N. & Mészáros, P. Gamma-Ray Bursts. *Science* **337**, 932 (2012). 1208.6522.
2. Kumar, P. & Zhang, B. The physics of gamma-ray bursts & relativistic jets. *Phys. Rep.* **561**, 1–109 (2015). 1410.0679.
3. Mészáros, P. Theories of Gamma-Ray Bursts. *ARA&A* **40**, 137–169 (2002). astro-ph/0111170.
4. Piran, T. The physics of gamma-ray bursts. *Reviews of Modern Physics* **76**, 1143–1210 (2004). astro-ph/0405503.
5. Mészáros, P., Razzaque, S. & Zhang, B. GeV-TeV emission from  $\gamma$ -ray bursts. *New A Rev.* **48**, 445–451 (2004).
6. Fan, Y.-Z. & Piran, T. High-energy  $\gamma$ -ray emission from gamma-ray bursts — before GLAST. *Frontiers of Physics in China* **3**, 306–330 (2008). 0805.2221.
7. Galli, A. & Piro, L. Prospects for detection of very high-energy emission from GRB in the context of the external shock model. *A&A* **489**, 1073–1077 (2008). 0805.2884.
8. Inoue, S. *et al.* Gamma-ray burst science in the era of the Cherenkov Telescope Array. *Astroparticle Physics* **43**, 252–275 (2013). 1301.3014.

- 412 9. Nava, L. High-energy emission from gamma-ray bursts. *International Journal of Modern*  
413 *Physics D* **27**, 1842003 (2018). 1804.01524.
- 414 10. Aleksić, J. *et al.* The major upgrade of the MAGIC telescopes, Part I: The hardware im-  
415 provements and the commissioning of the system. *Astroparticle Physics* **72**, 61–75 (2016).  
416 1409.6073.
- 417 11. Aleksić, J. *et al.* The major upgrade of the MAGIC telescopes, Part II: A performance study  
418 using observations of the Crab Nebula. *Astroparticle Physics* **72**, 76–94 (2016). 1409.5594.
- 419 12. Gropp, J. D. GRB 190114C: Swift detection of a very bright burst with a bright optical  
420 counterpart. *GRB Coordinates Network, Circular Service, No. 23688, #1 (2019/January-0)*  
421 **23688** (2019).
- 422 13. Hamburg, R. GRB 190114C: Fermi GBM detection. *GRB Coordinates Network, Circular*  
423 *Service, No. 23707, #1 (2019/January-0)* **23707** (2019).
- 424 14. Selsing, J. GRB 190114C: NOT optical counterpart and redshift. *GRB Coordinates Network,*  
425 *Circular Service, No. 23695, #1 (2019/January-0)* **23695** (2019).
- 426 15. Castro-Tirado, A. GRB 190114C: refined redshift by the 10.4m GTC. *GRB Coordinates*  
427 *Network, Circular Service, No. 23708, #1 (2019/January-0)* **23708** (2019).
- 428 16. Mirzoyan, R. First time detection of a GRB at sub-TeV energies; MAGIC detects the GRB  
429 190114C. *The Astronomer’s Telegram* **12390** (2019).



- 430 17. Dwek, E. & Krennrich, F. The extragalactic background light and the gamma-ray opacity of  
431 the universe. *Astroparticle Physics* **43**, 112–133 (2013). 1209.4661.
- 432 18. Domínguez, A. *et al.* Extragalactic background light inferred from AEGIS galaxy-SED-type  
433 fractions. *MNRAS* **410**, 2556–2578 (2011). 1007.1459.
- 434 19. Wang, Y., Li, L., Moradi, R. & Ruffini, R. GRB 190114C: A Gamma-ray Burst of Many faces.  
435 *arXiv e-prints* (2019). 1901.07505.
- 436 20. Ravasio, M. E. *et al.* GRB 190114C: from prompt to afterglow? *arXiv e-prints* (2019).  
437 1902.01861.
- 438 21. Ackermann, M. *et al.* The First Fermi-LAT Gamma-Ray Burst Catalog. *ApJS* **209**, 11 (2013).  
439 1303.2908.
- 440 22. Piran, T. & Nakar, E. On the External Shock Synchrotron Model for Gamma-ray Bursts’ GeV  
441 Emission. *ApJ* **718**, L63–L67 (2010). 1003.5919.
- 442 23. Ackermann, M. *et al.* Fermi-LAT Observations of the Gamma-Ray Burst GRB 130427A.  
443 *Science* **343**, 42–47 (2014). 1311.5623.
- 444 24. Kouveliotou, C. *et al.* NuSTAR Observations of GRB 130427A Establish a Single Component  
445 Synchrotron Afterglow Origin for the Late Optical to Multi-GeV Emission. *ApJ* **779**, L1  
446 (2013). 1311.5245.
- 447 25. Meszaros, P., Rees, M. J. & Papathanassiou, H. Spectral properties of blast-wave models of  
448 gamma-ray burst sources. *ApJ* **432**, 181–193 (1994). astro-ph/9311071.

- 449 26. Zhang, B. & Mészáros, P. High-Energy Spectral Components in Gamma-Ray Burst After-  
450 glows. *ApJ* **559**, 110–122 (2001). *astro-ph/0103229*.
- 451 27. Beniamini, P., Nava, L., Duran, R. B. & Piran, T. Energies of GRB blast waves and prompt  
452 efficiencies as implied by modelling of X-ray and GeV afterglows. *MNRAS* **454**, 1073–1085  
453 (2015). *1504.04833*.
- 454 28. CTA Consortium. *Science with the Cherenkov Telescope Array* (World Scientific Publishing  
455 Co, 2019).
- 456 29. Amati, L. *et al.* Intrinsic spectra and energetics of BeppoSAX Gamma-Ray Bursts with known  
457 redshifts. *A&A* **390**, 81–89 (2002). *astro-ph/0205230*.
- 458 30. Yonetoku, D. *et al.* Gamma-Ray Burst Formation Rate Inferred from the Spectral Peak Energy-  
459 Peak Luminosity Relation. *ApJ* **609**, 935–951 (2004). *astro-ph/0309217*.
- 460 31. Krimm, H. A. *et al.* GRB 190114C: Swift-BAT refined analysis. *GRB Coordinates Network*  
461 **23724**, 1 (2019).
- 462 32. Nava, L. *et al.* A complete sample of bright Swift long gamma-ray bursts: testing the spectral-  
463 energy correlations. *MNRAS* **421**, 1256–1264 (2012). *1112.4470*.
- 464 33. Vandenbroucke, J. GRB 190114C: Search for high-energy neutrinos with IceCube. *The As-*  
465 *tronomer’s Telegram* **12395** (2019).
- 466 34. Barthelmy, S. GCN capabilities and status, and the incorporation of LIGO/Virgo. In *APS*  
467 *Meeting Abstracts*, M13.004 (2016).

35. Carosi, A. *et al.* Recent follow-up observations of GRBs in the very high energy band with the MAGIC Telescopes. In Borisov, A. S. *et al.* (eds.) *34th International Cosmic Ray Conference (ICRC2015)*, vol. 34 of *International Cosmic Ray Conference*, 809 (2015).
36. Berti, A. & MAGIC GRB Group. Search for High Energy emission from GRBs with MAGIC. In *IAU Symposium*, vol. 324 of *IAU Symposium*, 70–73 (2017).
37. Fomin, V. *et al.* New methods of atmospheric Cherenkov imaging for gamma-ray astronomy. I. The false source method. *Astroparticle Physics* **2**, 137 – 150 (1994). URL <http://www.sciencedirect.com/science/article/pii/0927650594900361>.
38. Ahnen, M. L. *et al.* Performance of the MAGIC telescopes under moonlight. *Astroparticle Physics* **94**, 29–41 (2017). 1704.00906.
39. Fruck, C. *et al.* A novel LIDAR-based Atmospheric Calibration Method for Improving the Data Analysis of MAGIC. *ArXiv e-prints* (2014). 1403.3591.
40. Li, T. P. & Ma, Y. Q. Analysis methods for results in gamma-ray astronomy. *ApJ* **272**, 317–324 (1983).
41. Schmelling, M. The method of reduced cross-entropy A general approach to unfold probability distributions. *Nuclear Instruments and Methods in Physics Research A* **340**, 400–412 (1994).
42. Franceschini, A. & Rodighiero, G. The extragalactic background light revisited and the cosmic photon-photon opacity. *A&A* **603**, A34 (2017). 1705.10256.

- 486 43. Beardmore, A. The Swift-XRT WT mode spectrum of GRB190114C. *GRB Coordinates*  
487 *Network, Circular Service, No. 23736, #1 (2019)* **23736** (2019).
- 488 44. Nava, L., Sironi, L., Ghisellini, G., Celotti, A. & Ghirlanda, G. Afterglow emission in gamma-  
489 ray bursts - I. Pair-enriched ambient medium and radiative blast waves. *MNRAS* **433**, 2107–  
490 2121 (2013). 1211.2806.
- 491 45. Connaughton, V. & VERITAS Collaboration. Gamma-ray bursts at VERITAS energies. *As-*  
492 *troparticle Physics* **11**, 255–257 (1999).
- 493 46. Atkins, R. *et al.* Evidence for TEV Emission from GRB 970417A. *The Astrophysical Journal*  
494 **533**, L119–L122 (2000).
- 495 47. Atkins, R. *et al.* Limits on Very High Energy Emission from Gamma-Ray Bursts with the  
496 Milagro Observatory. *ApJ* **604**, L25–L28 (2004). astro-ph/0311389.
- 497 48. Abdo, A. A. *et al.* Milagro Constraints on Very High Energy Emission from Short-Duration  
498 Gamma-Ray Bursts. *ApJ* **666**, 361–367 (2007). 0705.1554.
- 499 49. Horan, D. *et al.* Very High Energy Observations of Gamma-Ray Burst Locations with the  
500 Whipple Telescope. *ApJ* **655**, 396–405 (2007). astro-ph/0701281.
- 501 50. Aharonian, F. *et al.* HESS Observations of the Prompt and Afterglow Phases of GRB 060602B.  
502 *ApJ* **690**, 1068–1073 (2009). 0809.2334.
- 503 51. Aharonian, F. *et al.* HESS observations of  $\gamma$ -ray bursts in 2003-2007. *A&A* **495**, 505–512  
504 (2009). 0901.2187.

- 505 52. Acciari, V. A. *et al.* VERITAS Observations of Gamma-Ray Bursts Detected by Swift. *ApJ*  
506 **743**, 62 (2011). 1109.0050.
- 507 53. H.E.S.S. Collaboration *et al.* Search for TeV Gamma-ray Emission from GRB 100621A, an  
508 extremely bright GRB in X-rays, with H.E.S.S. *A&A* **565**, A16 (2014). 1405.0488.
- 509 54. Alfaro, R. *et al.* Search for Very-high-energy Emission from Gamma-Ray Bursts Using the  
510 First 18 Months of Data from the HAWC Gamma-Ray Observatory. *The Astrophysical Journal*  
511 **843**, 88 (2017). 1705.01551.
- 512 55. Hoischen, C. *et al.* GRB Observations with H.E.S.S. II. *International Cosmic Ray Conference*  
513 **35**, 636 (2017). 1708.01088.
- 514 56. Abeysekara, A. U. *et al.* A Strong Limit on the Very-high-energy Emission from GRB  
515 150323A. *ApJ* **857**, 33 (2018). 1803.01266.
- 516 57. Albert, J. *et al.* MAGIC Upper Limits on the Very High Energy Emission from Gamma-Ray  
517 Bursts. *ApJ* **667**, 358–366 (2007). astro-ph/0612548.
- 518 58. Aleksić, J. *et al.* MAGIC observation of the GRB 080430 afterglow. *A&A* **517**, A5 (2010).  
519 1004.3665.
- 520 59. Aleksić, J. *et al.* MAGIC upper limits on the GRB 090102 afterglow. *MNRAS* **437**, 3103–  
521 3111 (2014). 1311.3637.
- 522 60. Ghirlanda, G. *et al.* Short gamma-ray bursts at the dawn of the gravitational wave era. *A&A*  
523 **594**, A84 (2016). 1607.07875.

61. Perley, D. A. *et al.* The Swift Gamma-Ray Burst Host Galaxy Legacy Survey. I. Sample Selection and Redshift Distribution. *ApJ* **817**, 7 (2016). 1504.02482.

62. Evans, P. A. *et al.* The Swift Burst Analyser. I. BAT and XRT spectral and flux evolution of gamma ray bursts. *A&A* **519**, A102 (2010). 1004.3208.

**Acknowledgements** We want to dedicate this paper to the memory of Eckart Lorenz. With his innovative spirit, infinite enthusiasm and vast knowledge of experimental methods, techniques and materials he played a key role in optimisation of the design of MAGIC, specifically for the GRB observations. We would like to thank the Instituto de Astrofísica de Canarias for the excellent working conditions at the Observatorio del Roque de los Muchachos in La Palma. The financial support of the German BMBF and MPG, the Italian INFN and INAF, the Swiss National Fund SNF, the ERDF under the Spanish MINECO (FPA2015-69818-P, FPA2012-36668, FPA2015-68378-P, FPA2015-69210-C6-2-R, FPA2015-69210-C6-4-R, FPA2015-69210-C6-6-R, AYA2015-71042-P, AYA2016-76012-C3-1-P, ESP2015-71662-C2-2-P, FPA201790566REDC), the Indian Department of Atomic Energy, the Japanese JSPS and MEXT and the Bulgarian Ministry of Education and Science, National RI Roadmap Project DO1-153/28.08.2018 is gratefully acknowledged. This work was also supported by the Spanish Centro de Excelencia “Severo Ochoa” SEV-2016-0588 and SEV-2015-0548, and Unidad de Excelencia “María de Maeztu” MDM-2014-0369, by the Croatian Science Foundation (HrZZ) Project IP-2016-06-9782 and the University of Rijeka Project 13.12.1.3.02, by the DFG Collaborative Research Centers SFB823/C4 and SFB876/C3, the Polish National Research Centre grant UMO-2016/22/M/ST9/00382 and by the Brazilian MCTIC, CNPq and FAPERJ.

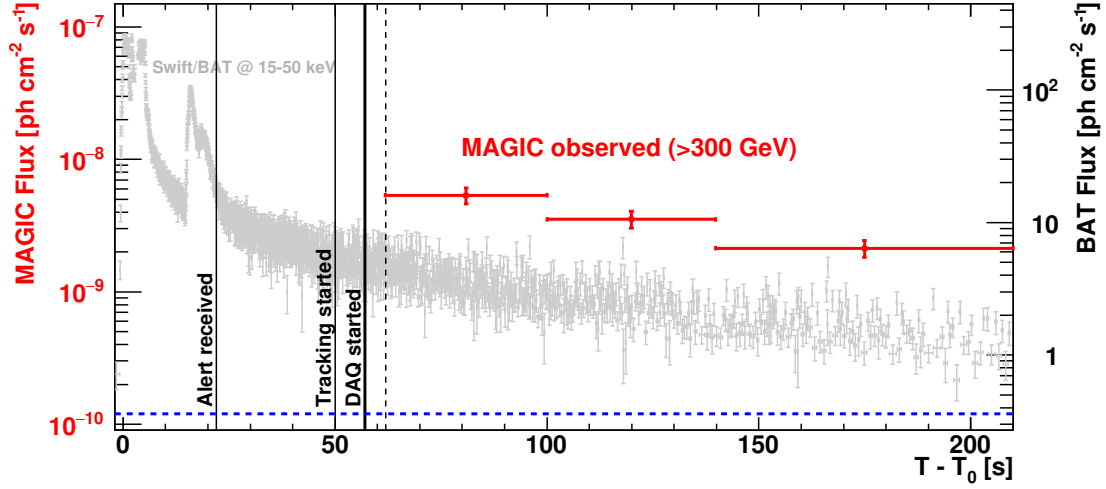
**Competing Interests** The authors declare that they have no competing financial interests.

**Author Contributions**

The MAGIC telescope system was designed and constructed by the MAGIC Collaboration. Operation, data processing, calibration, Monte Carlo simulations of the detector, and of theoretical models, and data analyses were performed by the members of the MAGIC Collaboration, who also discussed and approved the scientific results. All MAGIC collaborators contributed to the editing and comments to the final version of the manuscript. Susumu Inoue and Lara Nava coordinated the interpretation of the VHE data and together with Stefano Covino wrote the corresponding sections. Koji Noda and Alessio Berti, coordinated the analysis of the MAGIC data and together with Elena Moretti contributed to the writing of the relevant sections. Ievgen Vovk and Davide Miceli contributed to the calculation of limits, excesses and to the curves in fig. 3. Razmik Mirzoyan contributed in structuring and editing this paper.

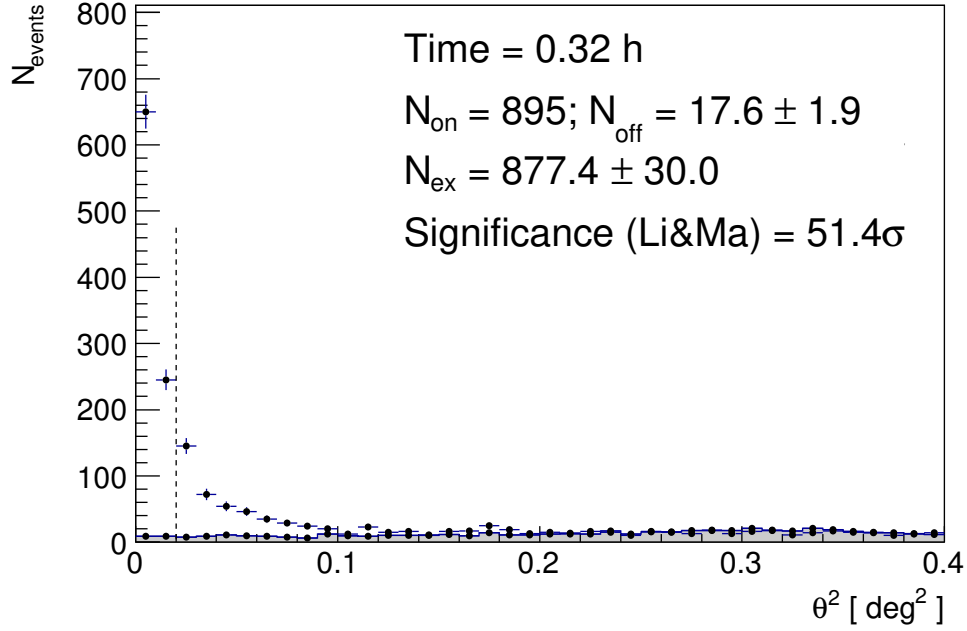
**Correspondence**

Correspondence and requests for materials should be addressed to MAGIC (email: [magic@mpp.mpg.de](mailto:magic@mpp.mpg.de)).



Extended Data Figure 1: **Light curves in the TeV and keV bands between  $T_0+62$  seconds and  $T_0+210$  seconds for GRB 190114C.** Light curve above 0.3 TeV in photon flux measured by MAGIC (red), compared with that between 15 keV and 50 keV measured by *Swift*/BAT<sup>62</sup> (grey) and the photon flux above 0.3 TeV of the Crab Nebula (blue dashed line). Vertical lines indicate the times for MAGIC when the alert was received ( $T_0 + 22$  s), when the tracking of the GRB by the telescopes started ( $T_0 + 50$  s), when the data acquisition started ( $T_0 + 57$  s), and when the data acquisition system became stable ( $T_0 + 62$  s, dotted line).





Extended Data Figure 2: **Significance of the gamma-ray signal between  $T_0+62$  seconds and  $T_0+1227$  seconds for GRB 190114C.** Distribution of the squared angular distance  $\theta^2$  for the MAGIC data (points) and background events (grey shaded area).  $\theta^2$  is defined as the squared angular distance between the nominal position of the source and the reconstructed arrival direction of the events. The dashed vertical line represents the value of the cut on  $\theta^2$ . This defines the signal region, where the number of events coming from the source ( $N_{\text{ON}}$ ) and from the background ( $N_{\text{OFF}}$ ) are computed.

Time bin	Energy flux	Spectral index
[ seconds after $T_0$ ]	[ erg cm <sup>-2</sup> s <sup>-1</sup> ]	
62 - 100	$[ 5.45 \pm 0.86 \text{ (stat)}^{+3.13}_{-2.59} \text{ (sys)} ] \cdot 10^{-8}$	$-1.90^{+0.36}_{-0.40} \text{ (stat)}^{+0.12}_{-0.21} \text{ (sys)}$
100 - 140	$[ 3.22 \pm 0.65 \text{ (stat)}^{+1.78}_{-1.42} \text{ (sys)} ] \cdot 10^{-8}$	$-2.15^{+0.43}_{-0.48} \text{ (stat)}^{+0.25}_{-0.32} \text{ (sys)}$
140 - 210	$[ 1.86 \pm 0.36 \text{ (stat)}^{+1.04}_{-0.88} \text{ (sys)} ] \cdot 10^{-8}$	$-2.31^{+0.47}_{-0.54} \text{ (stat)}^{+0.15}_{-0.22} \text{ (sys)}$
210 - 361.5	$[ 7.43 \pm 1.62 \text{ (stat)}^{+3.84}_{-4.79} \text{ (sys)} ] \cdot 10^{-9}$	$-2.53^{+0.53}_{-0.62} \text{ (stat)}^{+0.22}_{-0.24} \text{ (sys)}$
361.5 - 800	$[ 3.04 \pm 0.69 \text{ (stat)}^{+1.43}_{-1.11} \text{ (sys)} ] \cdot 10^{-9}$	$-2.41^{+0.51}_{-0.65} \text{ (stat)}^{+0.27}_{-0.34} \text{ (sys)}$
800 - 2454	$[ 4.97 \pm 2.50 \text{ (stat)}^{+2.38}_{-2.21} \text{ (sys)} ] \cdot 10^{-10}$	$-3.10^{+0.87}_{-1.25} \text{ (stat)}^{+0.75}_{-0.24} \text{ (sys)}$

Table 1: **Energy flux between 0.3 and 1 TeV in selected time bins for GRB 190114C.** Values are listed corresponding to the light curve in Figure 1. For each time bin, columns represent a) start time and end time of the bin; b) EBL-corrected energy flux in the 0.3-1 TeV range; c) best-fit spectral photon indices.

Event	redshift	$T_{\text{delay}}$ (s)	Zenith angle (deg)
GRB 061217	0.83	786.0	59.9
GRB 100816A	0.80	1439.0	26.0
GRB 160821B	0.16	24.0	34.0
GRB 190114C	0.42	58.0	55.8

Table 2: **List of GRBs observed under good technical and weather conditions by MAGIC with  $z < 1$  and  $T_{\text{delay}} < 1$  h.** The zenith angle at the beginning of the observations is reported in the last column. All except GRB 061217 were observed in stereoscopic mode. GRB 061217, GRB100816A and GRB 160821B are short GRBs, while GRB 190114C is a long GRB. Observations for a few other long GRBs with the same criteria were also conducted but are not listed here, as they were affected by technical problems or adverse observing conditions.